

## Biographies of the Authors



**Lev V. Eppelbaum** received M.Sc. from the Azerbaijan Oil Academy in 1982, and Ph.D. from the Geophysical Institute of Georgia in 1989. In 1982–1990 he worked as geophysicist, Researcher and Senior Researcher at the Institute of Geophysics in Baku (Azerbaijan). In 1991–1993 Eppelbaum completed postdoctoral studies in the Department of Geophysics and Planetary Sciences at Tel Aviv University; at present he occupies a position of Associate Professor at the same Department. He author of more than 300 publications including 5 books, 115 articles and 50 proceedings. His scientific interests cover potential and quasi-potential

geophysical field analysis, integrated interpretation of geophysical fields, geodynamics and tectonics. Eppelbaum's research interests in geothermics include examination of temperature regime of boreholes, thermal interactions at a depth, near-surface temperature measurements, study of climate of the past and nonlinear analysis.



**Izzy M. Kutasov** holds Ph.D. in Physics from O. Schmidt Earth Physics Institute in Moscow. He was a Senior Lecturer at the School of Petroleum Engineering, University of New South Wales, Sydney, and a graduate faculty member at the Department of Petroleum Engineering and Geosciences, Louisiana Tech University. He worked for Shell Development Co., Houston, as a Senior Research Physicist. Now Dr. I.M. Kutasov is a consultant with BYG Consulting Co., Boston, USA. His research interests include the temperature regime of deep wells, transient pressure/flow analysis, well drilling in permafrost areas as well as deriving climate of the past from subsurface temperature measurements. He is author of more than

250 publications including four books and more than 100 articles. Dr. Kutasov presented his scientific achievements at more than 60 International Conferences. His developments in the thermal data analysis in oil and gas wells received a wide recognition in the world scientific and engineering community.



**Arkady N. Pilchin** has been involved in geoscientific research since he received his M.Sc. in Physics in 1973. He participated in a number of geophysical and geological research endeavors including geothermal investigations in the Caucasus, Caspian Sea and Middle Asia, developing physical-geological models of the regions, earthquake prognosis, methods of prognosis for overpressure, analysis of the thermodynamic conditions of the Earth's crust, and those of oil and gas fields. He authored a number of geothermal methods including determining heat absorbing and heat releasing

strata within a sedimentary layer. After leaving the former USSR in 1990, he worked on geoscientific problems of different regions of the world such as the Eastern Mediterranean, Alps, Baltic Shield and Canada. He is the author of over 150 publications, including 2 books, 3 book chapters, several geothermal maps and 15 patents. His current scientific interests are related to the formation, evolution and thermodynamic conditions of: the magma-ocean, early Earth atmosphere, earliest lithosphere, water-ocean, ore deposits, and different generations of sulfur.

# Appendix A

## Computing Water Flow Geodynamics in Stratified Liquids (An Example from the Dead Sea Basin)

The Dead Sea (DS), with a total area of 1,049 km<sup>2</sup> is located on the border between Israel and Jordan. It is the lowest place on Earth (in 2013 it was about 427 m below the Mediterranean Sea level) with an arid climate (in the summer the temperature can reach 45 °C). Thermal and pressure parameters in this area are characterized by a strong inhomogeneity (Eppelbaum et al. 1996). The density of water in the vertical direction varies from 1,150 kg/m<sup>3</sup> at the DS surface up to 1,430 kg/m<sup>3</sup> at a depth of 310–330 m. This density gradient exceeds the normal water density gradient in the Earth's oceans and seas by more than 10<sup>2</sup>. Thus, the DS Basin may be considered a distinctive native polygon of vertically stratified liquid (the role of rock stratification in the magma-ocean was shown in Sect. 6.1). The most significant source of this are temperature and density gradients based on the constant inflow of a mineral substance from great depths (apparently, from the upper mantle). To analyze the water flows geodynamics in the DS Basin, solutions for the motion of stratified liquid with different initial boundary values can be used. Given the very high current rate of change of the physical, chemical and geological features of this unique basin, the development of a geodynamic predictable model of the area is extremely important. As was shown earlier, density practically always has a reliable correlation with temperature.

### A.1 Nature of the Problem

At present, the distinctive DS water is intensively utilized for extracting useful components contained in the liquid. This industrial activity, combined with the extremely arid climate has caused a significant drop in the sea level and the development of hundreds of sinkholes on the DS coast (Eppelbaum et al. 2008). For the DS, the conventional mathematical model describing sea behavior consists of a set of algebraic and a system of differential equations (e.g., Asmar and Ergenzinger 2002). The state of the sea is found by solving a system of ordinary differential equations formed by writing a system of mass balance equations for the water and eight major chemicals in the sea. The law of conservation is accounted for implicitly through evaporation calculations. However, this approach is unable to calculate all the peculiarities of the unique DS Basin. Interesting results were

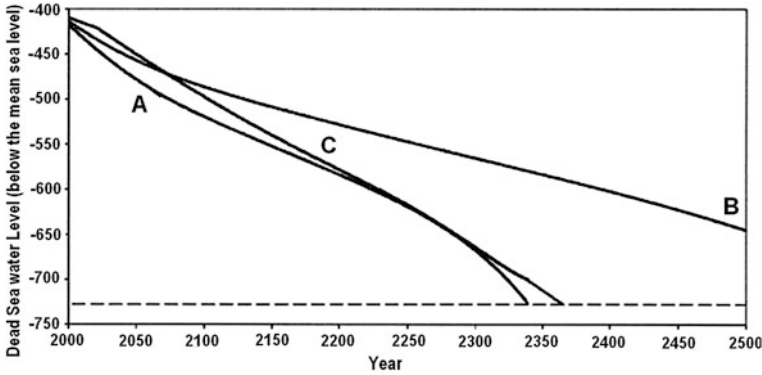


**Fig. A.1** Predicted water levels in the Dead Sea up to the year 2500. **a** Scenario 1 shows a continuation of the current conditions. **b** Scenario 2 shows cessation of industrial extraction activity. **c** Scenario 3 shows simplified climate change (after Asmar and Erdenzinger 2004)

presented by Bubnov and Linden (1998) for a homogeneously rotating linear density-stratified fluid. However, this approach demands significant evaluation.

We suggested applying a more precise physical-mathematical model which has implications for forecasting environmental scenarios for the DS (three variants are presented in Fig. A.1) and in estimating the possible ecological impact of excavation of a channel between the Red and Dead Seas (the differences in chemical composition of water from these seas are shown in Table A.1).

### A.2 Development of Mathematical-Physical Model

Let’s consider the motion of stratified, rotating and compressible liquid (*SRCL*) in the Cartesian coordinates  $(x_1, x_2, x_3)$  which is rotating together with the *SRCL*. Let’s assume that *SRCL* is rotating around axis  $Ox_3$  and Coriolis vector  $\mathbf{f} = (0, 0, f)$ , where  $f$  is the double angle velocity of rotation. *SRCL* is stratified along the axis  $Ox_3$ ; i.e., its density in undisturbed conditions depends on  $x_3$ ,  $\rho_0 = \rho_0(x_3)$ . We assume below that  $\rho_0(x_3) = Ae^{-2\beta x}$ ,  $A > 0, \beta > 0$ . Small *SRCL* motions under the influence of gravity acceleration without any external forces may be described as (Gabov and Sveshnikov 1986):

$$\begin{cases} \rho_0(x_3) \frac{\partial \mathbf{v}}{\partial t} + \rho_0(x_3) [\mathbf{f}, \mathbf{v}] + \nabla p + \mathbf{e}_3 \rho_1 g = 0, \\ \frac{\partial \rho_1}{\partial t} + (\mathbf{e}_3 \cdot \mathbf{v}) \rho'_0(x_3) + \rho_0(x_3) \operatorname{div} \mathbf{v} = 0, \\ \frac{\partial}{\partial t} \rho_1 = \frac{1}{c^2} \frac{\partial}{\partial t} p + \rho_0(x_3) \omega_0^2(x_3) \frac{(\mathbf{e}_3 \cdot \mathbf{v})}{g}, \end{cases} \quad (\text{A.1})$$

where  $g$  is the gravity acceleration,  $\mathbf{v} = (v_1, v_2, v_3)$  is the vector of *SRCL* particle motion,  $\rho_1$  is the change in *SRCL* density caused by its motion,  $c$  is the acoustic velocity,  $p$  is the dynamic pressure and  $\mathbf{e}_3$  is the ort of axis  $Ox_3$  and  $[\mathbf{f}, \mathbf{v}]$  denotes the vector product between two vectors. Value  $\omega_0^2(x_3) \geq 0$  is the quadrate of

**Table A.1** Some typical chemical analyses of the Dead Sea (*DS*) and the Red Sea (*RS*) (after Abu-Khader 2005; Ravizky and Nadav 2007, with supplements)

Element	<i>DS</i> concent-rations (mg/l)	<i>RS</i> concent-rations (mg/l)	Ratio, <i>DS/RS</i>
Chloride	224,000	23,000	9.74
Magnesium	44,000	1,500	29.33
Sodium	40,100	12,500	3.21
Calcium	17,650	500	35.3
Potassium	7,650	500	15.3
Bromide	5,300	70	75.71

Vyasyalay-Brent frequency. The condition  $\omega_0^2(x_3) \geq 0$  indicates an absence of convective motion and stability of the density distribution  $\rho_0(x_3)$  in the *SRCL*. It is known that physical parameters such as liquid density, acoustic velocity and pressure depend on temperature. Thus, the temperature is present in the formulas in an implicit form.

After several cumbersome transformations, Eq. (A.1) was reduced to the following type:

$$\frac{\partial^2}{\partial t^2} \left[ \frac{\partial^2 u}{\partial t^2} - c^2 \Delta_3 u + (f^2 + \beta^2 c^2) u \right] - \left[ \omega_0^2 c^2 \Delta_2 u + f^2 c^2 \frac{\partial^2 u}{\partial x_3^2} - \beta^2 c^2 f^2 u \right] = 0, \tag{A.2}$$

where  $u$  is a scalar function on which unknown functions  $\mathbf{v}$ ,  $\rho_1$  and  $p$  depend.

A generalization of Eq. (A.2) was investigated in Yakubov (1989). Let's consider the following problem

$$\left\{ \begin{aligned} L(t, D_t, D_x)u(t, x) &= \frac{\partial}{\partial t^2} \left[ \frac{\partial^2 u(t, x)}{\partial t^2} - \sum_{i,j=1}^3 \frac{\partial}{\partial x_i} \left( A_{ij}(t, x) \frac{\partial u(t, x)}{\partial x_j} \right) \right. \\ &\quad \left. + \sum_{i=1}^3 B_i(t, x) \frac{\partial u(t, x)}{\partial x_i} + C(t, x)u(t, x) \right] + \sum_{i,j=1}^3 \frac{\partial}{\partial x_i} \left( a_{ij}(t, x) \frac{\partial u(t, x)}{\partial x_j} \right) \\ &\quad \left. + \sum_{i=1}^3 b_i(t, x) \frac{\partial u(t, x)}{\partial x_i} + d(t, x)u(t, x) = f(t, x), \quad (t, x) \in [0, T] \times \Omega, \right. \end{aligned} \right. \tag{A.3}$$

where  $t$  is the time,  $A_{ij}$ ,  $B_i$ ,  $C$ ,  $a_{ij}$ ,  $b_i$ ,  $d$  are sufficiently smooth functions (for an application, see Eq. (A.2), and depend on  $c$ ,  $f$ ,  $\beta$  and  $\omega_0$ ).

$$u(t, x)|_{x \in \partial\Omega} = 0, \quad t \in [0, T], \tag{A.4}$$

$$\frac{\partial^k u(t, x)}{\partial t^k} \Big|_{t=0} = u_k(x), \quad k = 0, \dots, 3, \quad x \in \Omega. \tag{A.5}$$

Equations (A.4) and (A.5) present the Dirichlet boundary condition and the Cauchy initial conditions, respectively. Thus, Eqs. (A.3)–(A.5) can be seen as a foundation for the development of a geodynamical model of *SRCL* in the DS Basin (Yakubov and Eppelbaum 2005).

### **A.3 Application of the Methodology**

In the DS Basin (at the sea surface and at various depths) the following physical parameters were observed: temperature, gravity acceleration, water density, pressure, and acoustic velocity. Modern processing schemes can extend analytical continuations (downward, upward and sideward) of the physical observations to areas where we do not have these measurements. Thus, we can create a solvable system of differential equations and utilize this to create a precise physical-mathematical-geological model of the DS Basin. This model may be used not only for predictions, but also for the projected channel between the Red and Dead Seas, as well as to calculate the free electrochemical energy released from the unique DS Basin.

# Appendix B

## Water Production Using the Air-Cooling Method

The coastal regions in many regions of the world are characterized by their high moisture content—more than 15.0 g of water vapor per m<sup>3</sup> of air. This appendix is based on a phenomenon observed in the atmospheric boundary layer known as dew formation. At night, the boundary layer of air cools down considerably, which generally causes moisture saturation in the boundary layer and dew formation on the ground and plants. The ancient Greeks used this for water production (Zibold 1905). In more modern times, many investigations have been carried out to evaluate the quantitative potential of dew (Broza 1979; Kogan and Trahtman 2003; Nilsson 1996; Schemenauer and Cereceda 1992). However, all of these investigations have indicated that its potential is low.

To obtain fresh water by cooling humid air, we propose using a horizontal pipe. At the entrance to the pipe we will install a ventilator, which will introduce external humid air into the pipe. The outside wall of the pipe will be supplied with a special cooling system. A simplified scheme of this pipe is presented in Fig. B.1.

Let's consider the climatic conditions of Israel for illustrative purposes. According to Goldreich (2003) the average daily temperature, pressure and relative humidity in the coastal regions are  $\bar{T} = 25^\circ\text{C}$ ,  $\bar{P} = 1,004\text{ mb}$  and  $\bar{R}_H = 72\%$ , respectively. Preliminary calculations using a relatively simplified thermodynamics method based on these average values show that if the air is cooled to  $20^\circ\text{C}$ , 5.4 g of water can be obtained from 1.0 m<sup>3</sup> of air. If the radius of the pipe (cooling equipment) is 10 m and the velocity of the air inflow is 3.0 m/s, the air mass entering the pipe equals about 940 m<sup>3</sup>/s. Therefore, the maximum amount of water obtainable from this system is 5.0 l/s; i.e., about 430 m<sup>3</sup> per day and 78,000 m<sup>3</sup> per summer period. These rough estimates indicate that the idea of producing considerable amounts of drinking water by air-cooling in the coastal regions of Israel is practical.

Let's make some preliminary calculations for conditions typical to Israel. Based on these data, one can compute the daily average specific saturating humidity by applying Tetens's (1930) empirical formula:

$$\bar{Q}_s(\bar{P}, \bar{T}) = \frac{3.8}{\bar{P}} \bar{E} \cdot \exp\left\{17.27 \frac{\bar{T} - 273.16}{\bar{T} - 35.86}\right\}, \quad (\text{B.1a})$$

where  $\bar{T}$  is the absolute average temperature.

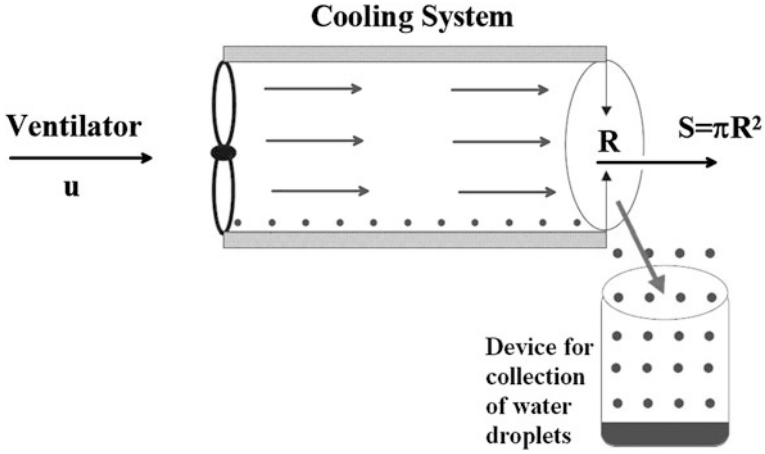


**Fig. B.1** Schematic diagram of pipe for water production (after Tzivion and Eppelbaum 2004)

$$\bar{Q}_S(\bar{P} = 1,004 \text{ mb}, \bar{T} = 298.16 \text{ }^\circ\text{C}) = 19.63 \times 10^{-3} \text{ g/g.} \quad (\text{B.1b})$$

Thus, under these conditions, 1 kg of air contains 19.63 g of water vapor. Hence, we can calculate the daily average specific humidity in summer:

$$\bar{q}_v(\bar{P}, \bar{T}) = \bar{Q}_S(\bar{P}, \bar{T}) \cdot RH \% = 14.13 \text{ g/kg.}$$

If the air is cooled down to 20 °C, the specific moisture content will remain unchanged, and only  $\bar{Q}_S$  will change, and its new value will be

$$\bar{Q}_S(\bar{p} = 1,004 \text{ mb}, \bar{T} = 278.16) = 5.4 \text{ g/kg.} \quad (\text{B.2})$$

Thus, we obtain the excessive water content—over saturation  $\Delta\bar{S}$ :

$$\Delta\bar{S} = \bar{q}_v - \bar{Q}_S = (14.13 - 5.4) = 8.73 \text{ g/kg.} \quad (\text{B.3})$$

The average air density  $\bar{\rho}$  for the above  $\bar{p}$  and  $\bar{T}$  values is roughly 1.2 kg/m<sup>3</sup>. Hence, we obtain

$$\Delta\bar{S} = 10.5 \text{ g/m}^3.$$

Thus, 1 m<sup>3</sup> of air contains excess water of about 10.5 g.

Now we estimate the maximum amount of water that can be obtained from this excess water in humid air. During vapor condensation, the following values will change:  $\bar{T}$ ,  $\bar{q}_v$ ,  $\bar{Q}_S(\bar{p}, \bar{T})$ ,  $\Delta\bar{S}$ .

We denote the new values of these functions as  $T^*$ ,  $P^*$ ,  $Q_S^*$  and  $\Delta S^*$ . For simplification we assume that due to condensation the pressure remains unchanged and that after condensation the over-saturation becomes zero. Under such conditions, we calculate the maximum possible amount of condensed water



$\delta M_{cond}$  (g/kg). If  $\delta M_{cond}$  of the water is condensed, after condensation  $T^*$ ,  $P^*$ ,  $q_v^*$ ,  $Q_S^*$  and  $\Delta S^*$  take on new values:

$$P^* = \bar{P}, T^* = \bar{T} + T', \quad q_v^* = \bar{q}_v - \delta M_{cond}, \quad Q_S^* = Q_S^*(\bar{P}, T^*). \quad (\text{B.4})$$

Here  $T'$  is the temperature disturbance due to condensation:

$$T' = \frac{L}{C_p} \delta M_{cond}, \quad (\text{B.5})$$

where  $L$  is the specific heat condensation, and  $C_p$  is the specific heat capacity of the air at a constant pressure.

For purposes of simplification, we introduce the following notations:

$$A = 3.8/P, \quad b = 17.27, \quad T_0 = 273.16, \quad C = 35.86.$$

According to (B.2), we obtain:

$$Q_S^*(\bar{P}, T^*) = A \cdot \exp\left(b \cdot \frac{\bar{T} - T_0 + T'}{\bar{T} - C + T'}\right) \quad (\text{B.6})$$

Given that  $T' \ll \bar{T}$ , we can rewrite (B.6) as follows:

$$Q_S^*(\bar{P}, T^*) = A \cdot \exp\left[b \frac{\bar{T} - T_0}{\bar{T} - C} + b \frac{T_0 - C}{(\bar{T} - C)^2}\right] T'. \quad (\text{B.7})$$

Using (B.2) and (B.5), we can rewrite  $Q_S^*$  as follows:

$$Q_S^*(\bar{P}, T^*) = \bar{Q}_S(\bar{P}, \bar{T}) \cdot \exp\left[\frac{b(T_0 - C)}{(\bar{T} - C)^2} \frac{L}{C_p} \delta M_{cond}\right]. \quad (\text{B.8})$$

Since the exponent is below unity, the final approximate value of  $Q_S^*$  is (Tzivion and Eppelbaum 2006):

$$Q_S^*(\bar{P}, T^*) \approx \bar{Q}_S(\bar{P}, \bar{T}) \cdot \exp\left[1 + \left(\frac{L}{C_p} b\right) \frac{T_0 - C}{(\bar{T} - C)^2} \delta M_{cond}\right]. \quad (\text{B.9})$$

Differentiating (B.2) with respect to  $\bar{T}$ , we obtain:

$$\frac{d\bar{Q}_S(\bar{P}, \bar{T})}{d\bar{T}} = \frac{b(T_0 - C)}{(\bar{T} - C)^2} \bar{Q}_S(\bar{P}, \bar{T}). \quad (\text{B.10})$$

Substituting (B.10) into (B.9), we obtain:

$$Q_S^*(\bar{P}, T^*) = \bar{Q}_S(\bar{P}, \bar{T}) + \frac{L}{C_p} \cdot \delta M_{cond} \frac{d\bar{Q}_S(\bar{P}, \bar{T})}{d\bar{T}}. \quad (\text{B.11})$$

Using (B.11) and taking into account that  $\Delta S^* = q_v^* - Q_S^* = 0$  and  $\bar{\Delta S} = \bar{q}_v - \bar{Q}_S$ , we obtain

$$\Delta\bar{S} - \left[ 1 + \frac{L}{C_p} \cdot \frac{d\bar{Q}_S(\bar{P}, \bar{T})}{d\bar{T}} \right] \delta M_{cond} = 0.$$

Hence we finally derive a formula for determining the maximum possible amount of condensed water:

$$\delta M_{cond} = \frac{\Delta\bar{S}}{A(\bar{P}, \bar{T})}, \quad (\text{B.12})$$

where

$$A(\bar{P}, \bar{T}) = \left[ 1 + \frac{L}{C_p} \cdot \frac{d\bar{Q}_S(\bar{P}, \bar{T})}{d\bar{T}} \right]. \quad (\text{B.13})$$

In the case of  $\bar{Q}_S(\bar{P}, \bar{T}) = 5.4 \text{ g/kg}$ ,  $b = 17.27$ ,  $\bar{T} = 278.16^\circ\text{C}$ ,  $L = 600 \text{ cal/g}$ ,  $C_p = 0.24 \text{ cal/g} \cdot \text{grad}$  we obtain:

$$A(\bar{p}, \bar{T}) = 1.942. \quad (\text{B.14})$$

Since  $\Delta\bar{S} = 8.73 \text{ g/kg}$ , we get that the maximum possible amount of condensed water will be about 4.5 g per 1 kg of air, i.e.

$$\delta M_{cond} \approx 4.5 \text{ g/kg} \quad \text{or} \quad \delta M_{cond} \approx 5.4 \text{ g/m}^3.$$

At  $\delta M_{cond} \approx 4.5 \text{ g/kg}$  based on Eqs. (B.2)–(B.5) and (B.9) we get that new values of  $T^*$ ,  $q_v^*$ ,  $Q_S^*$  and  $RH \%^*$  are equal to (Tzivion and Eppelbaum 2006):

$$T^* = 289.4^\circ, \quad q_v^* = 9.63 \text{ g/kg}, \quad Q_S^* = 9.63 \text{ g/kg}, \quad RH \%^* = 100\%. \quad (\text{B.15})$$

If we place a horizontal pipe with internal cooling in the vicinity of the sea coast perpendicularly to the latter, the amount of air entering the pipe will equal

$$M_{air} = U \cdot \rho_{air} \cdot S, \quad (\text{B.16})$$

where  $M_{air}$  is the mass of the air entering the pipe with an area  $S = \pi R_s$ ,  $U$  is the air velocity at the entrance to the pipe (m/s),  $\rho_{air}$  is the air density ( $\text{kg/m}^3$ ).

If we assume that  $R_s = 10$ ,  $U = 3 \text{ m/s}$ , and  $\rho = 1.2 \text{ kg/m}^3$ , then, according to (B.16), the mass of air entering the pipe in 1 s equals

$$M_{air} = 3.0(\text{m/s}) \cdot 1.2 (\text{kg/m}^3) \cdot 3.14 \cdot 100 \text{ m}^2,$$

$$M_{air} \approx 1,130 \text{ kg/s} = 942 \text{ m}^3/\text{s},$$

$$M_{air} \approx 940 \text{ m}^3/\text{s}.$$

Since it is possible to obtain 5.4 g of water from  $1 \text{ m}^3$  of air, the maximum amount of water obtainable from this system roughly amounts to 5,000 g of water in 1 s; i.e., about 18,000 kg of water per hour, or about  $430 \text{ m}^3$  per day and  $78,000 \text{ m}^3$  per summer period.

These rough estimates show that producing a considerable amount of water by air cooling is feasible. The obtained water can be used for drinking and other purposes. It should be noted that this methodology could be applied in Israel and in many regions of world at the sea coasts with high humidity.

## References

- Abu-Khader MM (2005) Viable engineering options to enhance the NaCl quality from the Dead Sea in Jordan. *J Cleaner Prod* 14(1):80–86
- Asmar BN, Ergenzinger P (2002) Dynamic simulation of the Dead Sea. *Adv Water Resour* 25:263–277
- Asmar BN, Ergenzinger P (2004) The Dead Sea is unlikely to dry up in 50 years. *EOS* 85(7):69–73
- Broza M (1979) Dew, fog and hygroscopic food as a source of water for desert arthropods. *J Arid Environ* 2:43–49
- Bubnov BM, Linden PF (1998) Diffusion stratification in a rotating linearly-stratified fluid. *Fluids Dyn* 33(2):201–208
- Eppelbaum LV, Modelevsky MM, Pilchin AN (1996) Geothermal investigations in the Dead Sea rift zone, Israel: implications for petroleum geology. *J Pet Geol* 19(4):425–444
- Eppelbaum LV, Ezersky MG, Al-Zoubi AS, Goldshmidt VI, Legchenko A (2008) Study of the factors affecting the karst volume assessment in the Dead Sea sinkhole problem using microgravity field analysis and 3D modeling. *Adv GeoSci* 19:97–115
- Gabov SA, Sveshnikov AG (1986) Problems of stratified liquid dynamics. Nauka, Moscow
- Goldreich Y (2003) The climate of Israel, observations, research and applications. Kluwer Academic Publication, NY
- Kogan B, Trahtman A (2003) The moisture from the air as water resource in arid region: hopes, doubts and facts. *J Arid Environ* 53:231–240
- Nilsson T (1996) Initial experiments on dew collection in Sweden and Tanzania. *Solar Energy Math Solar Cells* 40:23–32
- Ravizky A, Nadav N (2007) Salt production by the evaporation of SWRO brine in Eilat: a success story. *Desalination* 205:374–379
- Schemenauer RS, Cereceda P (1992) The quality of fog water collected for domestic and agricultural use in Chile. *J Appl Meteorol* 31:275–290
- Tetens O (1930) Ober einige meteorologische Vegriffe. *Z Geophys* 6:297–309
- Tzivion S, Eppelbaum L (2004) Water production using air cooling under the conditions of some coastal regions of world. In: *Trans of the 2nd international scient conference organized by the World Congress of Georgian Jews*. Bat Yam, Israel, pp 39–40
- Tzivion S, Eppelbaum L (2006) Water production using air-cooling under the conditions of some coastal regions of world. In: *Proceedings of the 1st international conference on from invitation and development to production, from research institute to the water industry*, Sde Boqer, Israel, pp 139–144
- Yakubov YS (1989) Correctness of one initial boundary value problem describing the motion of stratified liquid. *Izv AN Azerb. SSR (Baku, Azerbaijan)*, No 4–5, 21–27
- Yakubov YS, Eppelbaum LV (2005) Geodynamics of water flows in the Dead Sea basin: a proposed model for analysis of stratified, rotating and compressible liquid. In: *Proceedings of the 2nd EUG meeting*, vol 7(291), Vienna, Austria, pp 1–3
- Zibold EI (1905) The role of underground dew in water supply of Feodosia. *Trans of experimental forestries*, No 111, Sankt-Petersburg (in Russian)

# Index

## A

Abikh triangle, 201  
Abnormal gravity effect, 345  
Abnormally high porous pressure, 124  
Abnormally high stratum pressure (AHSP),  
119, 126, 133, 165, 203, 209, 220, 342  
Abnormally low stratum pressure, 125  
Acasta Gneiss complex, 280  
Accretion, 1, 7, 13, 20, 26, 34, 58, 137, 269,  
275  
Accretion of the Earth, 22  
Adelaide fold belt, 55, 64  
Adriatic Sea, 43  
Advanced wavelet, 711  
Aegean Sea, 43  
Alborz, 340  
Alpine-Himalayan orogenic belt, 351  
Alpine-Himalayan Seismotectonic belt, 464  
Anglo-Dutch Basin, 434  
Annual temperature variations, 632  
Annular materials, 492, 559  
Anoxic atmosphere, 317  
Anticline structure, 46, 129  
Appalachians, 56, 323, 351, 358  
Apsheron archipelago, 401, 405, 407, 428  
Arabian plate, 62  
Arabian Shield, 351  
Aralsor superdeep borehole, 50, 440  
Arava, 421  
Arbitrary function reconstruction, 659  
Archean craton lithosphere, 349  
Archean crust, 64, 323, 329  
Archean hydrosphere, 27  
Archimedes law, 272  
Arctic Coastal Plain, 263  
Arid climate, 735  
Ash Meadows area, 611  
Ashdod, 334  
Ashkelon, 334

Asphalt deposit, 631

Atlit, 334

Autocorrelation matrix, 623

Average daily temperature, 739

Axial heat flow, 183

## B

Baikal, 58, 323

Bakhar oil and gas deposit, 639

Baltic shield, 43, 54, 66, 351, 358, 359

Bårdsholmen, 11

Basaltic layer, 725

Basaltic magma, 188, 195, 200

Be'er-Sheva, 334

Beaufort Sea, 265, 546, 683

Beaufort-Mackenzie Basin, 54

Beilagan, 334, 404, 409, 433, 446

Berggren formula, 245

Bernoulli equation, 606

Bibi-Eybat, 401, 407

Binagady, 401, 407

Black Lake hydrocarbon deposit, 637

Black Sea, 43, 57, 73, 340, 646, 649

Black smokers, 163, 166, 183, 184

Borsunly, 409

Bottom edges of magnetized bodies (BEMB),  
333, 336

Bottom-hole circulating temperature (BHCT),  
478, 496, 499, 501, 502, 504, 506, 513

Bottom-hole mud temperature, 513

Boudouard reaction, 277, 282, 302

Bouguer gravity, 203, 699

Bragooni, 123

Branisko Mts, 11

Brazilian platform, 43

Bulla Island, 123, 201, 408

Buzovny, 401

Byerlee's law, 334

**C**

Camp Century, 655  
 Canadian Shield, 49  
 Carmel, 334  
 Cascade Range, 335  
 Caspian Sea, 43, 123, 129, 132, 202, 307, 340, 406, 411, 420, 428, 639  
 Central Alberta, 404  
 Central Anatolia, 335  
 Central Graben (North Sea), 515  
 Central Indian Ridge, 184  
 Central Pontides, 335  
 Central Turkmenistan, 134  
 Central Ventura Basin, 408, 435  
 Channel between the Red and Dead Seas, 736  
 Characteristic areal method, 454  
 Cherry Valley, 70  
 CO<sub>2</sub>, 112, 138, 167, 185, 200, 257, 279, 303, 415, 522  
 Coast Ranges, 335  
 Coefficient of informativity, 722  
 Coefficient of viscosity, 705  
 Compacton, 461  
 Compressibility, 107, 119, 124, 135, 191, 195, 202, 215, 309, 320, 416, 508, 614  
 Compressional velocity, 217, 695  
 Condensed water, 742  
 Conditional entropy, 717  
 Continental drift hypothesis, 18  
 Cordillera, 43  
 Coso geothermal field, 441  
 Crimea, 135, 430, 464  
 Cubic nonlinearity, 458  
 Curie point, 71, 331, 332, 336  
 Curie point depth (CPD), 331, 333, 336  
 Curie point of magnetite, 332  
 Curie point of titanomagnetite, 332

**D**

Dabie Shan, 11  
 Darcy equation, 99  
 Dead Sea, 334, 408, 422, 634  
 Death Valley, 172  
 Deccan traps region, 51  
 Decision making, 710  
 Dew formation, 739  
 Dharwar Craton, 53, 54, 67  
 Diablo Mountain range, 206  
 Diffusivity equation, 249, 487, 528, 597, 682  
 Dilatancy, 127, 134, 221, 223  
 Dilatancy theory of earthquake prediction, 127  
 Dixon Island, 283, 289

Dnieper-Donets depression, 53, 439  
 Dowletabad area, 123  
 Dry valley, 612  
 Duffing equation, 459  
 Duvanniy Sea, 123

**E**

Early Earth's atmosphere, 27, 34, 137, 140, 271, 279, 284, 288, 304, 305, 316, 325, 329  
 Early Earth's evolution, 281, 291, 297, 316, 327, 338  
 Early Earth's surface, 280, 285  
 Earth's climate, 655  
 Earth's differentiation, 12  
 Earth's evolution, 13, 25, 34, 60, 272, 280, 442  
 Earth's heat flow, 58  
 Earth's emitted radiation, 155  
 Eastern Desert, 62  
 Eastern-Kuban' depression, 411  
 East Pacific Rise, 184  
 Eilat, 705  
 Ein Yahav circular structure, 730  
 El Tatio Geysir Field, 178  
 Energetic effect, 257  
 Environmental scenario, 736  
 Equivalent static density, 512, 517  
 Error function, 395, 514, 665, 722  
 Evlakh, 406  
 Expert systems, 709  
 Extremely arid climate, 707  
 Eyjafjallajökull volcano, 173

**F**

Fennoscandian Shield, 47, 64  
 Fergana, 135, 430  
 Fergana depression, 412  
 Fe-rich magma, 272, 293, 321  
 Fictitious body, 455  
 Filizchay pyrite-polymetallic deposit, 635  
 Finite-localized structure, 461  
 Finnish Precambrian bedrock, 46  
 Banded iron formation (BIF), 13, 278, 287, 296, 297  
 Flash heating, 468  
 Flin Flon belt, 49  
 Fluid flow history, 493, 559  
 Fontaine de Vaucluse, 182  
 Fourier's law, 40, 99, 447, 597  
 Franciscan complex, 357  
 Frozen formations, 239, 249, 545, 561

Fumarole, 167, 170, 174, 178, 185, 220, 325  
 Fuzzy logic approach, 709

## G

Galilee, 334, 729  
 Ganja, 406, 433  
 Gawler craton, 55, 64  
 Gazanbulag, 409, 440, 446  
 Gazly (Uzbekistan) earthquakes, 468  
 Geodynamic events, 468  
 Geothermal gradient, 14, 37, 46, 71, 126, 152, 173, 292, 312, 325, 393, 405, 425, 440, 478, 494, 500, 513, 536, 559, 601, 631, 662, 679, 706  
 Giant Springs, 182  
 Glaciation periods, 657  
 Gold-sulphide deposit, Yakutiya, 634  
 Gorely Volcanic Center, 193  
 Gousany, 401, 407  
 Gran Paradiso, 363  
 Gravitational differentiation, 22  
 Great Australian Artesial Basin, 182  
 Greater Caucasus, 218, 339, 360, 424, 627, 629, 711, 725  
 Greenland, 282, 298  
 Grenville province, 55, 70, 358  
 Ground surface temperature history (GSTH), 659, 671, 672, 679  
 Gushkhana, 203

## H

Halilbağı region, 356  
 Halls Creek Orogen, 70  
 Hatchobaru geothermal field, 162  
 Hayan Kort, 123  
 Heat absorption, 51, 54, 411, 427, 431, 438, 443  
 Heat capacity, 28, 105, 202, 246, 295, 324, 393, 441, 484, 602, 606  
 Heat energy, 1, 19, 28, 41, 57, 109, 163, 181, 188, 202, 208, 269, 292, 324, 405, 431, 445, 613  
 Heat flow, 18, 35, 46, 54, 67, 155, 202, 203, 239, 247, 249, 259, 292, 306, 341, 393, 404, 426, 442, 480, 541, 581, 603, 623, 643, 661, 673, 699, 705  
 Heat flow density, 18, 36, 41, 44, 50, 239, 255, 325, 401, 427, 433, 596

Heat islands, 674, 677  
 Heat radiation, 22, 29, 295, 323  
 Hierarchical approach, 713, 715  
 Highly nonlinear phenomenon, 658  
 Horizontal geothermal gradient, 75, 419, 420, 426  
 Humble dome, 36  
 Humid air, 739  
 Hydraulic conductivity, 165, 610, 611

## I

Imperial Valley, 493  
 Indian shield, 323  
 Information-statistical methods, 711  
 Informativeness, 713  
 Ingushetiya, 467  
 Integrated interpretation, 711  
 Intermediate asymptotics, 461  
 Internal cooling, 742  
 Inverse correlation, 202, 456, 466, 623, 695, 707  
 Iron oxides, 8, 278, 297, 331, 346  
 Isostatic equilibrium, 211, 306, 353  
 Israel, 43  
 Isua supracrustal belt, 282, 288  
 Izu Peninsula, 466

## J

Jacobi elliptical function, 459  
 Jan Mayen, 318  
 Jędrzychowice, 356  
 Jigoku Geysir, 178  
 Juan de Fuca Ridge, 184

## K

Kaczawa Mts, 355  
 Kalmas area, 133  
 Kamchatka Peninsula, 161, 170, 181, 206  
 Kamchatka-Kuril Arc, 170  
 Kant-Laplace theory, 2  
 Karkeshet caldera, 729  
 Katekh pyrite-polymetallic deposit, 629  
 Katsdag pyrite-polymetallic deposit, 631, 725  
 Kerch-Taman, 210  
 Klyuchevskaya Sopka, 170  
 Kola Peninsula, 54, 431, 533, 656  
 Kola superdeep borehole, 50, 431, 656

Kopetdag, 340, 464  
 Kotelnikov's criterion, 723  
 Krivoi Rog, 430  
 Kura depression, 129, 397, 442, 723  
 Kurdamir, 424, 433  
 Kvaisa pyrite-polymetallic deposit, 628  
 Kyurovdag area, 133  
 Kyursangya area, 130  
 Kyzyl-Bulakh gold-pyrite deposit, 626

## L

Lake Baikal, 52, 446  
 Laplace equation, 39, 447, 675  
 Large igneous provinces (LIP), 187, 320  
 La Ronge domain, 11  
 Las Termas belt, 70  
 Lateral thermal conductivity, 36, 661, 673, 679  
 Lena River, 253  
 Lesser Antilles, 183  
 Lesser Caucasus, 362, 623, 723  
 Liaodong uplift, 67  
 Linguistic variables, 709  
 Lithosphere–asthenosphere boundary, 318  
 Lithospheric slab, 351  
 Lithospheric thickness, 320  
 Lithostatic pressure, 119, 126, 132, 187, 196, 275, 306, 312, 327, 338, 344, 348, 354  
 Localized wave, 458, 461  
 Lokbatan, 203, 401  
 Longitudinal thermal conductivity, 113  
 Long-lived radioactive elements, 12, 22, 46, 58  
 Long-lived radioactive isotopes, 1, 7, 20, 34, 58, 270, 323  
 Los Angeles Basin, 404, 415, 425  
 Low velocity zone (LVZ), 294, 319, 320  
 Luangwa rift, 43

## M

Mackenzie delta, 253, 523  
 Mafic volcanic complex, 349  
 Magma chambers, 110, 188, 199, 321  
 Magma-ocean, 1, 12, 13, 24, 65, 110, 137, 188, 269, 271, 273, 274, 286, 292, 299, 316, 321, 327, 328, 338  
 Mangyshlak, 135  
 Mantle temperature, 28, 195  
 Manzano Mountains, 70  
 Mapping submarine springs, 647

Marmara Sea, 42  
 Massada, 421  
 Mass balance equations, 733  
 Massive volcanic eruptions, 655  
 Mathematical model of glaciation, 657  
 Mean air temperature, 167, 256  
 Mean night thermal gradient, 468  
 Measurement errors, 709  
 Meliata, 356  
 Melting point, 11, 25, 72, 109, 112, 293, 327, 350  
 Messinian salinity crisis, 205  
 Meteoric water, 163, 166, 324, 707  
 Michigan Basin, 44, 408, 435, 437  
 Mid-Atlantic, 104, 184  
 Mid-Atlantic Ridge, 161, 185, 359  
 Middle Kura depression, 131, 333, 342, 405, 424, 438, 637, 725  
 Middle Urals, 619  
 Mid-ocean ridge, 183, 318, 359  
 Mid-ocean ridge basalts, 195, 274  
 Mineral barometer, 309  
 Mir-Bashir, 409  
 Mishovdag area, 133  
 Moho discontinuity, 71, 316, 323, 326, 349  
 Moisture content, 241, 246  
 Molten asthenosphere, 346  
 Monviso, 356  
 Moon's albedo, 32  
 Mounting-building process, 657  
 Mozambique belt, 11  
 Mud temperature, 477, 517, 524, 541, 575  
 Mud volcanoes, 56, 201, 205, 211, 214, 341  
 Muradkhanly area, 130  
 Muradkhanly oil deposit, 635  
 Mutnovsky Volcano, 170, 193

## N

Neckar Valley, 643  
 Neftechala, 409  
 Neftyanie Kammi, 401  
 Nevada, 335, 432, 611  
 Newtonian relationship, 478, 482  
 Non-climatic effects, 662  
 Nonequilibrium potential source, 463  
 Nonlinear diffusion, 462  
 Nonradiogenic component, 51  
 Nonuniform boundary conditions, 39  
 Normal distribution function, 709  
 Norris Geyser Basin, 162, 170

- North China Massif, 55  
 North East German Basin, 397  
 Northern Alaska, 263  
 Northern Arava Valley, 334, 421  
 Nupe Basin, 335
- O**
- Obducted oceanic lithosphere, 353  
 Oceanic lithosphere slab (OLS), 351, 353, 358  
 Oceanic mantle, 319  
 Oceanic peridotite layer, 351  
 Ocean island basalts, 59, 195  
 Octemberyan area, 428  
 Omission of target, 720  
 Ontario, 335  
 Optic temperature sensing, 152  
 Ordinary differential equation, 458, 465, 657  
 Organic matter, 413, 520, 663  
 Oslo Rift, 63, 64  
 Overpressure, 72, 119, 126, 189, 202, 211, 220, 221, 274, 306, 315, 327, 339, 347, 354, 412
- P**
- Pacific Ring of Fire, 170, 174, 178, 187, 205, 359, 463  
 Padar, 409  
 Paleozoic Appalachians, 64  
 Pannonian Basin, 43, 67, 323  
 Paratunka, 170, 181  
 Paris Basin, 414  
 Partial entropy, 718  
 Pascal's law, 207, 274, 327, 346  
 Passive remote sensing, 155  
 Penetration rate, 477, 481, 494, 560, 684  
 Permafrost, 35, 152, 240, 241, 246, 250, 255, 562, 564, 575, 662, 685  
 Petrological composition, 305, 396, 417  
 Phase transition, 127, 239, 245, 259, 466, 552, 560, 685, 701  
 Physical properties of rocks, 696  
 Pikwitonei granulite domain, 47  
 Pilbara Craton, 280, 282, 285, 288, 290, 338  
 Planetary differentiation, 137  
 Planetesimals, 3, 10, 20, 137, 270, 271  
 Plate tectonics, 464  
 Plume effect, 464  
 Poisson's equation, 447  
 Poisson's law, 710  
 Polarization vector, 456  
 Pragmatic component, 713  
 Pragmatic criterion, 715  
 Pre-Alpine basement, 725  
 Precaspian Basin, 340  
 Probability integral, 722  
 Production index, 415  
 Proterozoic Wopmay orogen, 64  
 Proto-Earth, 26  
 Protoplanetary disk, 7, 9  
 Prudhoe Bay, 251, 263, 546
- Q**
- Qinghai-Tibet plateau, 356, 365  
 Quseir, 335
- R**
- Radial distance, 488, 536, 552, 562, 677  
 Radioactive heat production, 46, 61  
 Ramat HaGolan, 334  
 Range province, 67, 333  
 Rapa, 412  
 Ras el 'Ain, 182  
 Real body, 455  
 Recharge zone, 163, 182, 324, 404, 608  
 Red Sea, 42, 50, 185, 335  
 Relative oil content, 136  
 Residual anomalous temperature map, 632  
 Resistance temperature detector, 152  
 Reykjanes Peninsula, 173  
 Rhyolitic magma, 199, 200  
 Ring structures, 730  
 Rio Maule River, 182  
 Risk of erroneous solution, 720  
 Rosh Pina, 334  
 Ruhr Basin, 70
- S**
- Saatly superdeep borehole, 402, 429, 725  
 Sakhalin, 135, 206, 210  
 Salt diapir, 204, 211, 220, 729  
 Salt dome, 37, 205, 424, 634, 699  
 Salton Sea, 408, 432, 437  
 Salton Trough, 44, 58, 403, 432  
 Sanbagawa metamorphic belt, 11  
 Sangachaly Sea, 123  
 San Joaquin Valley Basin, 413  
 Saxonian Granulite Mountains, 117  
 Schmidt-Lyttleton accretionary theory, 2  
 Schmidt's hypothesis, 23  
 Seasonal temperature variations, 157, 447, 467, 619, 705  
 Semantic criterion, 715  
 Sesia Zone, 356



- Seward Peninsula, 356  
 Shamkhor, 334, 406  
 Shear strength, 127, 222, 339  
 Sheki, 406, 466  
 Shemakha-Gobustan zone, 203  
 Shikabe Geyser, 178  
 Shock wave, 457, 460  
 Sierra Nevada, 48, 57, 360  
 Sierra Nevada batholith, 49  
 Simplon railway tunnel, 645  
 Sinai, 335, 729  
 Slag-dumps, 649  
 Slave Craton, 53, 67, 323  
 Sodom, 421  
 Solar system, 1, 7, 23, 29, 270, 293  
 South Caspian depression, 56, 340, 342, 403, 411, 425, 439  
 South Fork Mountain, 356  
 Space of the physical-geological factors, 723  
 Specific saturating humidity, 739  
 Staraya Matsesta, 57, 430  
 Statistical-probabilistic approach, 716  
 Stefan-Boltzmann law, 30, 33, 34  
 Stella Spring, 182  
 Stratified, rotating and compressible liquid, 736  
 Strongly nonlinear heat catalytic processes, 460  
 Structural function, 465  
 Sturm-Liouville nonlinear problem, 658  
 Subcontinental lithospheric mantle, 318  
 Sulu UHP belt, 335  
 Sun's radiation, 1, 28, 32, 325  
 Surakhany, 401  
 Surface formation temperature, 502  
 Suwa Geyser, 178  
 Switch wave, 458  
 Syntactic component, 713
- T**
- Takinoue geothermal area, 177  
 Taratashski, 430  
 Tarim Block, 55  
 Tatsumaki Jigoku, 177  
 Taupo Volcanic Zone, 175, 176  
 Temperature anomalous variations, 466  
 Temperature gradient, 36  
 Temperature moment, 455, 634, 640  
 Temperature-depth profile, 38, 659, 662, 673, 680  
 Terrain relief inclination, 455  
 Tersko-Sunzhensk depression, 135  
 Thawing regime, 239
- Theoretical errors, 709  
 Thermal balance condition, 250  
 Thermal catastrophe, 28  
 Thermal conductivity of ice, 698  
 Thermal diffusivity, 16, 113, 115, 393, 445, 529, 533, 539, 552, 561, 567, 577, 597, 644, 665, 679, 687  
 Thermal water, 15, 42, 162, 178, 180, 201, 324, 396, 423, 440, 593, 605  
 Thomson Belt, 55  
 Time-Temperature index, 414  
 Timna dome, 729  
 Total organic carbon, 414  
 Transformation of ferrous to ferric iron (TFFI), 10, 12, 13, 278, 298, 299, 303, 329, 332, 346  
 Trans-Hudson Orogen, 55, 67  
 Transition wave, 456, 463  
 Transversal thermal conductivity, 113  
 Tumen' province, 412  
 Tyrrhenian Sea, 43, 67
- U**
- Ukrainian Shield, 45, 49, 54, 55, 57, 301, 319  
 Ultra-high pressure, 211, 219, 315  
 Umi Jigoku, 177  
 Undisturbed formation temperature, 477, 484, 488, 539, 560, 564, 596, 602, 683  
 Unfrozen water, 239, 242, 246  
 Urals, 351, 355, 362, 411, 430  
 Urey ratio, 28, 65  
 Usami hot springs, 466  
 Usu volcano, 162
- V**
- Valles Caldera, 431, 432, 433, 438  
 Valley of Geysers, 161, 170, 172, 180, 181  
 Ventilation indices, 705  
 Vertical geothermal gradient, 73, 216, 398, 406, 419, 423, 426, 429, 441  
 Vertically stratified liquid, 735  
 Voltri massif, 356  
 Volume thermal expansion, 119, 125, 309, 343  
 Vostok station, 257  
 Vyasyalay-Brent frequency, 737
- W**
- Water flows geodynamics, 735  
 Wellbore fluid, 153, 480, 493  
 Wellbore formation, 252, 559, 582  
 Well stability, 241

Western Tianshans, 356  
Western Turkmenian depression, 123, 411,  
439, 440  
Whakarewarewa Thermal Valley, 175  
Wheatstone bridge circuit, 153  
White smokers, 162, 166, 183, 184  
Wilbur, 624  
Williston Basin, 408, 420, 425, 434

**Y**

Yakutia, 253, 412, 531, 633  
Yellowstone National Park, 167, 169, 180,  
188, 335

**Z**

Zahrat et Qurein, 729  
Zambezi rift, 43  
Zermatt-Saas, 356  
Zhangguangcailing terrane, 67  
Zirya, 401  
Zykh, 401, 407